A Smart Combined Wireless Sensor for Vibration and AE Signals Measurement

A Smart Combined Wireless Sensor Net for Vibration and AE Signals Measurement

Zhaoyu Zhang
State Key Laboratory of Electrical Insulation and Power Equipment
Xi'an Jiaotong University
Xi'an, China
Department of Electronics and Telecommunications
Politecnico di Torino
Turin, Italy
zhaoyu.zhang@polito.it

Luca Lombardo
Department of Electronics and Telecommunications
Politecnico di Torino
Turin, Italy
luca.lombardo@polito.it

Tianyi Shi
State Key Laboratory of Electrical Insulation and Power Equipment
Xi'an Jiaotong University
Xi'an, China
945827377@qq.com

Xutao Han
State Key Laboratory of Electrical Insulation and Power Equipment
Xi'an Jiaotong University
Xi'an, China
xutaohan@xjtu.edu.cn

Marco Parvis
Department of Electronics and Telecommunications
Politecnico di Torino
Turin, Italy
marco.parvis@polito.it

Junhao Li
State Key Laboratory of Electrical Insulation and Power Equipment
Xi'an Jiaotong University
Xi'an, China
junhaoli@mail.xjtu.edu.cn

***Abstract*—Mechanical and insulation defects can lead to severe faults in power equipment, making it crucial to conduct a comprehensive and accurate fusion diagnosis. Vibration and acoustic emission (AE) are two effective ways to detect the above two defects. This paper proposes a reliable smart vibration and AE combined wireless sensor featuring both low cost and low power consumption, which is suitable for real-time assessment of power equipment conditions. Initially, the sensor structure is designed and its feasibility is verified by simulation. Subsequently, a developed Printed Circuit Board (PCB) is integrated in the prototype which realizes data acquisition, storage, processing and transmission. Moreover, a fast impedance response self-calibration method based on pseudorandom binary maximum length sequence (M-sequence), is proposed with the aim of remotely calibrating the sensor in an efficient and convenient way. The sensor performance were assessed achieving very promising results. In particular, the vibration sensitivity is 510 mV/g and AE sensitivity exceeds 70 dB. The data rate surpasses 1 Mbps within 8 m range, and the life time can be at least one year. In addition, self-calibration consumes only 6.82 ms and it has a negligible power consumption. Finally, the vibration-partial discharge (PD) joint experiment demonstrates effective measurement capabilities of the sensor. The presented sensor, as an example of advanced industrial measurement, provides a smart solution for mechanical and insulation defects fusion detection.**

Keywords—smart wireless sensor, mechanical vibration, partial discharge, acoustic emission.

I. INTRODUCTION

Distributed measurement systems and Wireless Sensor Networks find application in several field such as smart home automation, public security and cultural heritage [1]. The large capabilities and flexibility of these systems are attracting an ever-growing attention of scholars. Nevertheless, few solutions are nowadays available for the continuous monitoring and detection of mechanical and insulation defects in power plants.

Mechanical and insulation defects are two significant reasons leading to serious fault of large power equipment such as gas insulated switchgear (GIS), transformer, generator, etc. [3], and any damage would be great once the fault occurs. Vibration and AE are usually measured to detect the mechanical and insulation defects with good performance, however, they are differently sensitive to some specific defect [7]. For instance, in GIS (Fig. 1), the metal particles generated by poor contact friction on grounded enclosure would cause vibration but associated with a very small Partial Discharge (PD) signal, while on basin insulator there would be a large PD signal but slight vibration due to the long distance from enclosure [11], so the characteristics and position of the defect determine which detection signal is more suitable.

The fusion measurement and analysis of multi-signal for equipment defect detection is an important study topic [12]. In [13] A. Stief, et al. analyzed acoustic, electric, and vibration signals gathered from induction motors operating under different conditions in order to diagnose both electrical and mechanical faults applying the fusion approach based on the combination of a two-stage Bayesian method and Principal Component Analysis (PCA). In [14] A. Secic et al. categorized and reviewed the state of the art of vibro-acoustic diagnostic methods for power transformers, concluding that fusion measurement will be promising with novel techniques. In [15] M. Khazaee et al. reported that vibration and acoustic signals processed by data fusion with the method based on D-S theory of evidence could increase the fault detection accuracy of planetary gearbox.

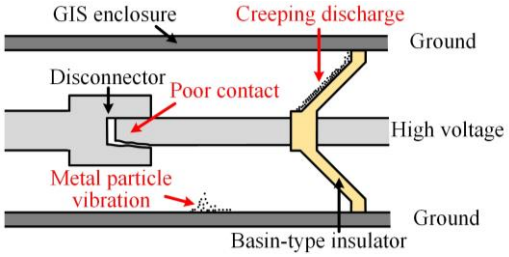

Fig. 1. The vibration and PD caused by metal particles in GIS .

Traditional measurement systems for defect and fault detection in power equipment is typically based on wired sensors and probes, which is impractical for on-field continuous monitoring. Moreover, they are usually based single signal measurement and analysis. As a result, the efficiency of industrial maintenance is very low. Nowadays, with the development of fourth industrial revolution, advanced measurement is currently evolving to be wireless, distributed, multi-signal, smart, and it makes extensive use of

fusion analysis. In [16], multiscale analysis of motor vibration and stator current signals is proposed as a deep-learning-based model named multiresolution & multisensor fusion network. In [17], a novel edge collaborative compressed sensing for mechanical vibration monitoring (MVM) is presented to address the severe shortage of storage and computational resources and long delay in transmitting massive vibration data in Wireless Sensor Net (WSN) for MVM. A novel intelligent diagnosis method based on Multisensor Fusion (MSF) and Convolutional Neural Network (CNN) is explored in [18]. Most researches focus on Artificial Intelligent (AI) algorithms, however, there are few reliable wireless combined sensor for evaluating power equipment condition.

Moreover, the problem of sensitivity calibration of piezoelectric sensors is usually underestimated in literature. Calibration might be implemented in laboratory with professional and bulky apparatus [19], but this might not be so convenient and, often, it is too expensive for industrial measurement.

Vibration or AE sensitivity curve of piezoelectric sensors is actually a kind of frequency response curve, which is related to the impedance response curve of the sensor. Generally, to acquire the impedance response curve, impedance analyzer is used with frequency sweep, which is time consuming.

For excitation signal, white noise is ideal since its power spectral density distributes uniformly over the entire frequency band, but it can be generated difficultly. To this aim, pseudorandom binary M-sequence, a periodic sequence owing similar probability properties with discrete binary white noise [21], can be used to get the impedance response curve of the designed sensor quickly and without the employment of expensive instrumentation.

In this paper, we dedicate to develop a smart combined wireless sensor for vibration and AE signals measurement, which could be used in mechanical and insulation defect detection in power equipment featuring at the same time low cost, very low power consumption and the capability to carry out a real-time monitor for long time periods without any maintenance. The sensor is designed and simulations are carried out to confirm its sensitivity, then its technical frame and main functions are implemented. To demonstrate its performances, a prototype is assembled and several tests about vibration and AE sensitivities, data rate and energy consumption are carried out. A method to implement on-board sensor impedance response calibration by using M-sequence is implemented as well in order to reduce maintenance cost over long-time on-field monitoring. Finally, the sensor is used to measure the vibration and AE signals of vibration - PD joint experiment.

II. Development of The Sensor Net

The proposed sensor is composed by different elements including a piezoelectric transducer and an electronic board which is able to acquire and process data from the transducer, and transmitting them by using Bluetooth Low-Energy (BLE).

A. Mechanical Design

Since piezoelectric vibration sensor share the same structure with piezoelectric AE sensor, and they work at different bands, it is possible to make a combined sensor by scientific design, which output signal includes both vibration (under 2 kHz) and AE (above 20 kHz) information. The proposed sensor is shown in Fig. 2.

The acoustic matching layer increases acoustic transmissivity for AE measurement and works as base for vibration measurement. The PZT-5 element realizes the conversion from vibration and AE to voltage due to its excellent piezoelectric property. The backing plate is able to decrease the noise from echo and broaden AE response band, and it is embedded in a metal mass which offers inertia for vibration measurement. Furthermore, a PCB is mounted inside the sensor consisting of analog processing circuit, microcontroller with integrated Bluetooth Low-Energy (BLE) transceiver, RF antenna and matching networks. The electronic system is responsible for self-calibration, ADC measuring, analog and digital data processing, on-board data storage and RF data transmission.

To verify the feasibility of the sensor and confirm its response parameters, a Finite Elements Analysis (FEA) is employed to calculate the sensitivity of vibration and AE. The physical parameters are determined by theoretical calculation and set in simulation [22].

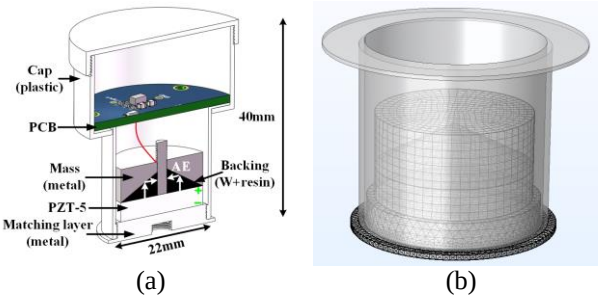

Fig. 2. The sensor structure. (a) Structure design. (b) FEA model.

Since the sensor is designed for defect detection of GIS, the vibration and AE measurement bands should be 100 Hz ~ 2 kHz and 20 kHz ~ 100 kHz. The results of simulation are shown in Fig. 3. It is possible to see that vibration sensitivity reaches 55 mV/g under 2 kHz (Fig. 3 (a)). The high frequency response is hopping in Fig. 3 (b): AE sensitivity increases up to 84 dB at 43 kHz (resonant frequency) and drops down to 50 dB at 70 kHz as well as 44 dB at 86 kHz. Therefore, the sensor is able to properly acquire both vibration and AE signals at the same time.

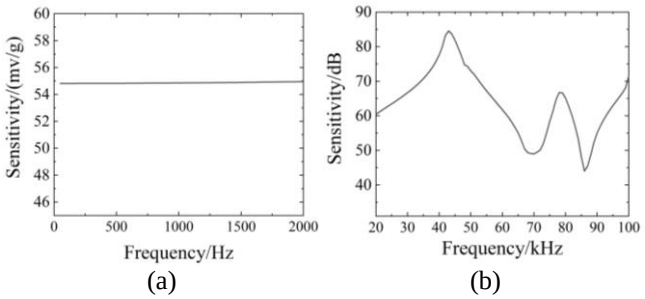

Fig. 3. The simulation results. (a) Vibration sensitivity. (b) AE sensitivity.

B. Electronic Design

The technical frame of the sensor is described in Fig. 4. The BLE system-on-chip (EFR32MG24, Silicon Labs) is the core part of the PCB which enables the sensor to acquire and store data, calibrate itself, implement edge computing and RF communication with BLE 5.3 protocol. The chip provides high-performing ADC and DAC peripherals together with a very low power consumption and a large computing capability, making it an ideal choice for high-performing

sensing applications. During a measurement, the analog signal from PZT-5 is processed and then converted to digital signal by ADC, after storage and computing, it is transmitted by the BLE transceiver. For self-calibration, the DAC generates M-sequence signal on PZT-5 through a matching resistor (50 Ω), simultaneously, the signal on PZT-5 is acquired by measurement flow. Actually, the M-sequence signal is stored in the chip memory, and it is identical for each calibration.

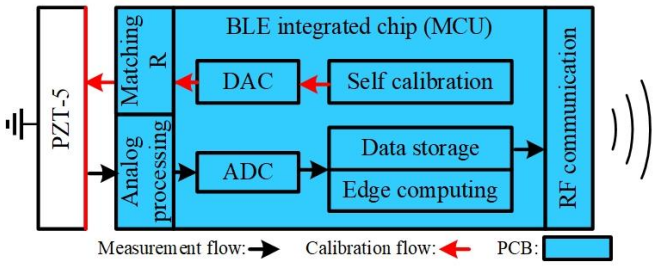

Fig. 4. Technical frame of the proposed sensor.

The sensor is controlled by a dedicated remote Bluetooth Client (PC, smart phone, etc.). The PCB of the prototype is shown in Fig. 5 (a), and it has a diameter of 33 mm. Since the sensor is supplied by 3V coin cell battery (CR2477), the static input signal of ADC should be shifted to half of supply (around 1.5V) in order to acquire bipolar signals from the piezoelectric sensor. Besides, the high impedance of PZT-5 should be converted to low in order to avoid unacceptable signal degradation. A simple analog processing circuit is designed for this purpose, as shown in Fig. 5 (b).

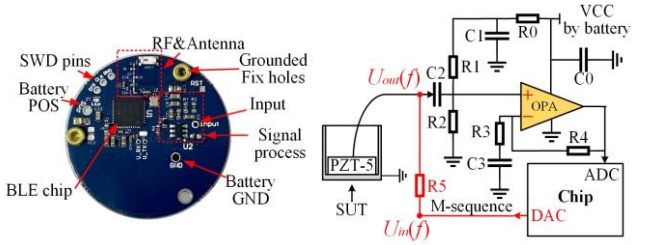

(a) (b)

Fig. 5. PCB design. (a) The PCB. (b) Analog processing circuit (black) and self calibration (red) circuit.

In particular, R0, C1 are used to stabilize the voltage which supplies the operational amplifier (OPA), and a middle-rail voltage (about VCC/2) is obtained by means of a simple voltage divider (R1, R2) to realize the required DC shift. C2 blocks the DC component from the sensor. R4 and R3 determine the signal gain (set to 5 in this paper). R5 works as matching resistor for impedance response self-calibration. All component values are displayed in TABLE I.

TABLE I. ANALOG PROCESSING CIRCUIT PARAMETERS

Component	Value	Component	Value
R0	1 kΩ	C0	200 μF
R1	10 MΩ	C1	100 μF
R2	10 MΩ	C2	10 μF
R3	50 kΩ	C3	10 μF
R4	200 kΩ	R5	50 Ω

C. Self-Calibration

The impedance self-calibration flow (red line) is shown in Fig.5 (b), Pseudorandom M-sequence, as $U_{in}(f)$, can be generated by the DAC directly on the microcontroller and applied through a matching resistor (50 Ω) to the PZT-5. Meanwhile, the ADC is employed to acquire the $U_{out}(f)$. It is noted the M-sequence measurement band can be set up by adjusting its clock frequency. Since 100 Hz ~ 100 kHz is our calibration band, the clock frequency (f_{cp}) should be 300 kHz according to M-sequence measurement bandwidth (f_m) equation [21]:

$$f_m \approx \frac{f_{cp}}{3} \tag{1}$$

Fig. 6 (a) demonstrates the normalized input and output calibration signals. Impedance response curve $S(f)$ could be calculated by Eq. (2), where f is the specific frequency, $U_{out}(f)$ and $U_{in}(f)$ represent the voltage amplitudes of the output and input, respectively.

$$S(f) = 20 \times \log_{10} \frac{U_{out}(f)}{U_{in}(f)} \tag{2}$$

It is depicted in Fig. 6 (b) that the impedance response curves measured by frequency sweep method and M-sequence method match very well, although the latter is characterized by some fluctuations.

The time consumed by frequency sweep method is 1 min for 120 samples, however, M-sequence method requires only 6.823 ms for 500 samples. On the other hand, the energy consumed by M-sequence method is very low, which makes this approach very suitable for self-calibration on battery-powered BLE wireless sensors. The obtained impedance response curve could be used to reflect the output response change caused by dielectric characteristic change [23].

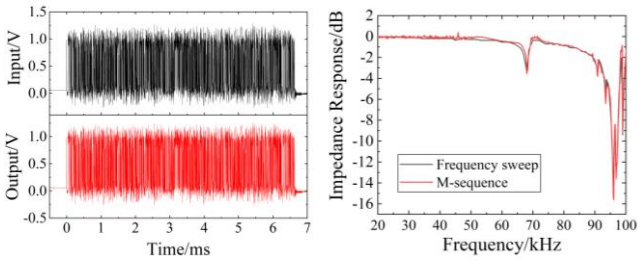

(a) (b)

Fig. 6. Self-calibration implementation. (a) The input and output signals (normalization). (b) Calibration result.

D. Digital Signal Processing and Communication

The sensor also supports edge computing based on 32-bit ARM Cortex-M33. The statistical analysis, such as FFT, Wavelet Transform, etc, could be achieved if these algorithms are wrote in advance and embedded in the firmware. In this paper, the self-calibration program is coded inside, so that the sensor can be calibrated remotely when required. In addition, for wireless transmission, the data rate of the sensor could be 2 Mbps theoretically. Since the digital signal processing and communication are executed by the integrated chip with BLE 5.3, these operations require few energy. The current consumption of Microcontroller Unit (MCU) is tens of milliamperes, and that of radio is 8 mA at most according to the chip datasheet. On the other hand, the duration of these operations is short, so the power consumption would be few enough for achieving a long operative life.

Transducer electronic data sheet (TEDS) is also an important feature for smart sensors, therefore, any primary information about the sensor can be directly saved in the flash memory of the microcontroller, so that the TEDS can be remotely accessible under BLE connection and used to properly correct the acquired data. these will be read after the Bluetooth connection. The measured data are temporarily saved in RAM and, then, transferred to remote client when a connection is established.

The complete assembled prototype is shown in Fig. 7. It is featured by:

1) Simultaneous collection of vibration and AE signals.
2) BLE 5.3 with battery supply (CR 2477, 1 A·h).
3) Data rate can be set up to 2 Mbps (1.35 Mbps is practical).
4) 32-bit ARM Cortex®-M33 core and MCU peripherals could realize edge computing and self-calibration.

(a) (b)

Fig. 7. Smart vibration-AE combined wireless sensor. (a) The sensor (without cap). (b) Manufactured sensor.

III. Performance Test

A. Vibration and AE Calibration

The vibration and AE calibration platforms employed in the work are established according to ISO 12714:1999 and ISO 16063-21:2003 respectively in Fig.8 (a) and (b). (RS means Reference Sensor, SUT means Sensor Under Test)

The calibration results are shown in Fig.8 (c) and (d). Vibration sensitivity reaches around 510 mV/g, while AE sensitivity fluctuates between 70 dB ~ 90 dB and the lowest value is 71.5 dB at 95 kHz.

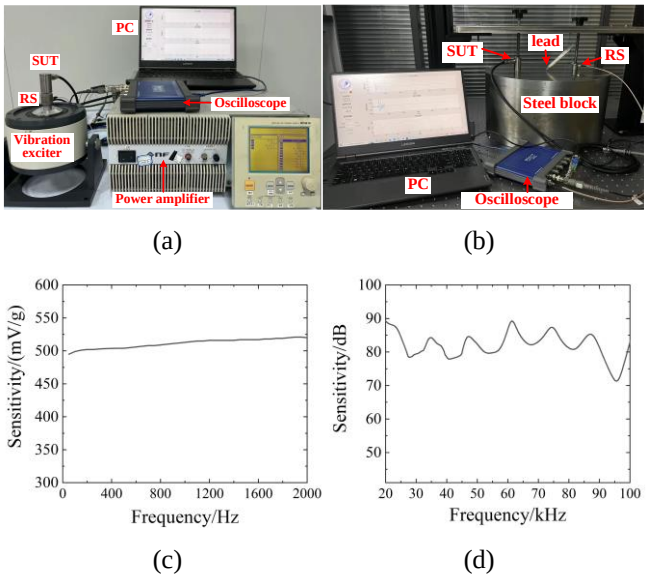

Fig. 8. Calibration experiment. (a) Vibration calibration. (b) AE calibration. (c) Vibration sensitivity. (d) AE sensitivity.

B. Data Rate

The performance of data rate is of paramount importance for measurement, especially for real time applications. There are several factors affecting data rate of the wireless sensor, environment and distance are two main factors. The proposed sensor works with BLE 5.3 which supports 2 Mbps data rate, The prototype is tested indoor and outdoor as the distance between the sensor and client increases from 1 m up to 20 m. Effective data rates tested are reported in TABLE II.

TABLE II. Data Rate Test

Distance	Data Rate	
	Indoor	***Outdoor***
1 m	1.35 Mbps	1.31 Mbps
4 m	1.17 Mbps	1.05 Mbps
8 m	1.1 Mbps	1.01 Mbps
12 m	1.058 Mbps	887.5 kbps
16 m	653.2 kbps	545.2 kbps
20 m	565.7 kbps	344.8 kbps

It is clear that the data rate reduces as the distance increases weather indoor or outdoor. In particular, indoor data rate reaches 1.35 Mbps at 1 m, and it decreases down to roughly 1.1 Mbps as the distance comes to 8 m. A similar trend is obtained outdoor, but with a slightly lower data rate. Anyway, the sensor is able to transmit at a data rate higher than 1 Mbps when client distance is lower than 8 m, a distance more than suitable for periodic fault detection of power equipment in industrial plants.

Even though the complete data processing can be carried out on-board by the microcontroller, at the moment, the data processing algorithm is implemented on the client. Therefore, the sensor node has to send over the BLE connection all the raw acquired data. A standard measurement data set will consists of about 50 k samples (16 bit per sample) which requires about 0.8 s to be transmitted at a data rate of 1 Mbps, which added to the measurement time of about 0.1 s results in a total time of less than 2 s for carrying out a complete measurement. This time is extremely shorter than the time required by standard test procedures, which requires also a wired setup and the periodic deployment of sensors and probes. The proposed sensor, instead, can be permanently deployed on the power equipment (also thanks to its low cost) and activated remotely performing a complete measurement in few seconds.

C. Energy Consumption

Energy consumption is also an important parameter for wireless sensors, since it affects the battery life and, therefore, the interval between sensor maintenance. The microcontroller has several optimized modes for reducing power consumption, moreover, the firmware is designed so that it remains in sleeping mode for most of time reducing the current to few microampere. Periodically, the chip awakes for BLE advertisement taking current impulses of about 10 mA within a very short time. A higher power consumption is expected during RF transmission. The authors decide to employ a direct way to measure the current as shown in Fig. 9. The voltage on a 1 Ω shunt resistor cascaded between battery and PCB is employed to perform the current measurement.

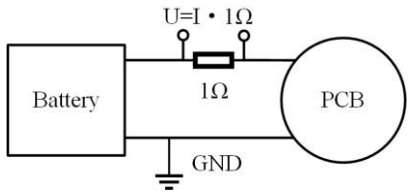

Fig. 9. The current measurement diagram.

The energy consumption of the sensor node includes advertisement, connection event, ADC measurement, DAC self-calibration and RF transmission. The current measured during each operation is shown in Fig. 10. However, in order to estimate the battery life, the charge is used to describe energy consumption, charge cost of each operation could be calculated by Eq. (3):

$$Q = \int_0^t idt \tag{3}$$

Therefore, it is easy to estimate the charges during the different events: advertisement Q_{adv}, connection event Q_{Con}, per ADC measurement Q_{adc}, per DAC self-calibraion Q_{dac} and per RF data transmission Q_{RF}. The estimated values are respectively 24 μC for Q_{adv}, 2 μC for Q_{Con}, 17.25 mC for Q_{RF}. While the Q_{adc} and Q_{dac} are negligible (0.1 μC and 0.6 μC respectively).

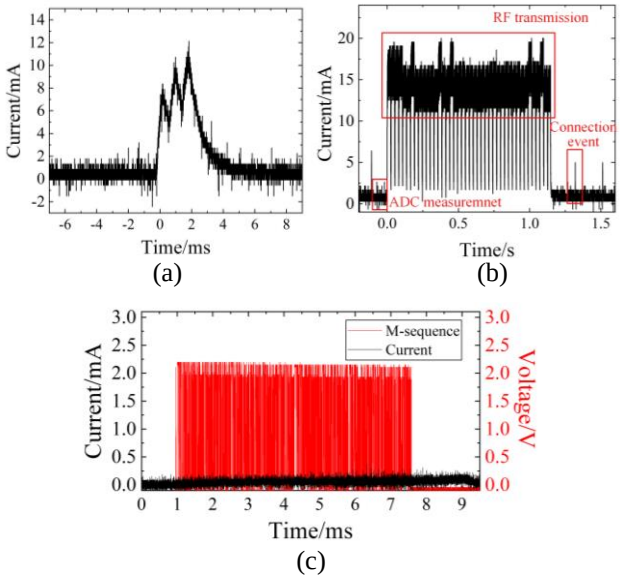

Fig. 10. Currents of the five main operations. (a) Advertisment. (b) ADC measurement, RF data transmission and connection event. (c) DAC.

For monitoring mode with fastest data rate set, if the sensor advertises every 10 s and makes one measurement every 10 min. The estimated charge per hour Q_{1h} would be:

$$Q_{1h} = n_{adv} \times Q_{adv} + n_{Con} \times Q_{Con} + 6 \times Q_{RF} \tag{4}$$

where n_{adv} and n_{Con} represent the numbers of advertisement and connection event per hour. Thus, the Q_{1h} is about 112.26 mC. Since the battery CR 2477 has a capacity of 1 A·h (3600C), the theoretical working duration would be estimated to be around 4 years. However, considering a real situation, the operative life is lower than this value due to battery self-discharge and capacity reduction for environmental parameters, but working life of about 1 year is practical. After this time, it is convenient to change the battery.

IV. Experiment

The vibration and PD joint experiment is carried out to verify performance of the sensor on the field. The experiment platform is shown in Fig. 11.

The experimental setup is arranged to simulate the real situation which could occur in a GIS. There is a pot with a high voltage electrode and ground plane, AC high voltage source is used to provide high electrical field for stimulating PD, and a vibration exciter for generating vibration. Several metal particles, as a kind of typical PD defect, are put in the SF_6 pot with a pressure of 0.4 MPa for insulation. The sensor is fixed on the ground of pot to measure signal.

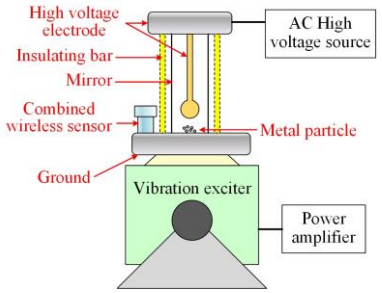

Fig. 11. Vibration - PD joint experiment.

When the voltage rises up more than 13 kV, the metal particles start to jump due to attraction of high voltage source, when particles fall back to the ground, the discharge happens to generate the PD signal.

Fig. 12 shows the output signal from proposed combined wireless sensor. There are some PD pulses on sine-like vibration. It is clear that the signal has different bands, therefore, the two main components are separated by digitally filtering the acquired signal obtaining vibration signal and PD signal by respectively a low pass (cut-off: 3 kHz) and a high pass (cut-off: 15 kHz) digital filters.

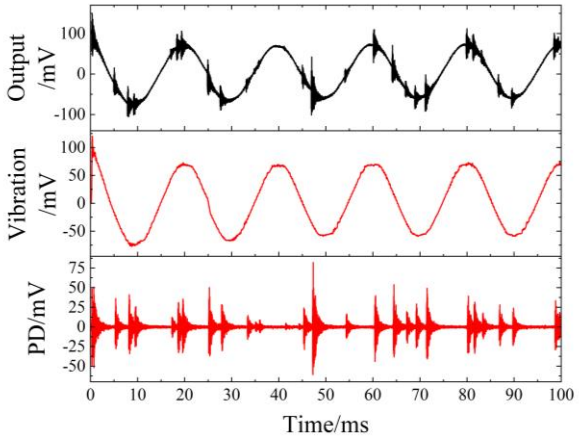

Fig. 12. Experiment result.

These results demonstrates that the proposed sensor is able to properly collect both vibration and AE signals simultaneously, which can be used for fusion analysis of insulation and mechanical defects in power equipment.

V. Conclusion

This article develops a novel wireless and smart vibration-AE combined sensor intended for mechanical and insulation defects detection of power equipment. The sensor is composed by a piezoelectric transducer coupled with a

dedicated acquisition circuit. The designed PCB achieves main functions as self-calibration, analog processing, edge computing, BLE transmission and data storage.

Several experimental tests were carried out to assess the effective performance of the proposed prototype, indicating that vibration sensitivity is 510 mV/g and AE sensitivity exceeds 70 dB; data rate keeps above 1 Mbps within 8 m distance wherever indoor or outdoor. Energy consumption is tested and operative life is estimated as 1 year at least. And the proposed M-sequence method for impedance response self-calibration costs only 6.82 ms and negligible power consumption. Furthermore, the vibration and PD joint experiment results confirm the effective measurement performance of the sensor.

The proposed sensor features very low power consumption and long operative life which, together with the intrinsic low cost of the device, make the sensor suitable for on-field continuous real-time monitoring of power equipment. Several sensors can be deployed on the field to and form a WSN for distributed non-destructive testing and fusion analysis. Future work will includes more experimental validation and the implementation of digital data processing directly on-board the sensor. This would contribute to further reduce power consumption and dramatically decrease the amount of data to be transmitted.

ACKNOWLEDGMENT

The authors would like to express their appreciation for financial supports from National Natural Science Foundation of China Joint Fund Key Project under Grant U22B20118.

REFERENCES

[1] Majid M, Habib S, Javed A R, et al. Applications of wireless sensor networks and internet of things frameworks in the industry revolution 4.0: A systematic literature review. Sensors, 2022, 22(6): 2087.

[2] Lombardo L, Parvis M, Corbellini S, et al. Environmental monitoring in the cultural heritage field. The European Physical Journal Plus, 2019, 134: 1-10.

[3] C. -J. Chou and C. -H. Chen, "Measurement and analysis of partial discharge of high and medium voltage power equipment," 2018 7th International Symposium on Next Generation Electronics (ISNE), 2018, pp. 1-4.

[4] M. Ren, C. Zhang, M. Dong, Z. Xiao and A. Qiu, "Partial discharges triggered by metal-particle on insulator surface under standard oscillating impulses in SF6 gas," in IEEE Transactions on Dielectrics and Electrical Insulation, vol. 22, no. 5, pp. 3007-3018, October 2015.

[5] J. Hao, Y. Ding, Y. Li, X. Li, X. Jiang and H. Peng, "Comparative Analysis of Partial Discharge and Mechanical Vibration Characteristics under Loose Bus Base with Foreign Body Defect of GIS," 2022 IEEE International Conference on High Voltage Engineering and Applications (ICHVE), 2022, pp. 1-4.

[6] S. Bagheri, Z. Moravej and G. B. Gharehpetian, "Classification and Discrimination Among Winding Mechanical Defects, Internal and External Electrical Faults, and Inrush Current of Transformer," in IEEE Transactions on Industrial Informatics, vol. 14, no. 2, pp. 484-493, Feb. 2018.

[7] H. D. Ilkhechi and M. H. Samimi, "Applications of the Acoustic Method in Partial Discharge Measurement: A Review," in IEEE Transactions on Dielectrics and Electrical Insulation, vol. 28, no. 1, pp. 42-51, February 2021.

[8] Y. -B. Wang et al., "Acoustic localization of partial discharge sources in power transformers using a particle-swarm-optimization-route-searching algorithm," in IEEE Transactions on Dielectrics and Electrical Insulation, vol. 24, no. 6, pp. 3647-3656, Dec. 2017.

[9] M. Iorgulescu, R. Beloiu and M. O. Popescu, "Vibration monitoring for diagnosis of electrical equipment's faults," 2010 12th International Conference on Optimization of Electrical and Electronic Equipment, 2010, pp. 493-499.

[10] Y. Shi, S. Ji, F. Zhang, Y. Dang and L. Zhu, "Application of Operating Deflection Shapes to the Vibration-Based Mechanical Condition Monitoring of Power Transformer Windings," in IEEE Transactions on Power Delivery, vol. 36, no. 4, pp. 2164-2173, Aug. 2021.

[11] X. Li, W. Liu, D. Ding and Y. Xu, "Metal Particle Movement and Induced Insulator Flashover Under Impact Vibration Generated By Switching Operation in GIS," in IEEE Transactions on Power Delivery, vol. 38, no. 2, pp. 757-766, April 2023.

[12] T. Xie, X. Huang and S. -K. Choi, "Intelligent Mechanical Fault Diagnosis Using Multisensor Fusion and Convolution Neural Network," in IEEE Transactions on Industrial Informatics, vol. 18, no. 5, pp. 3213-3223, May 2022.

[13] A. Stief, J. R. Ottewill, J. Baranowski and M. Orkisz, "A PCA and Two-Stage Bayesian Sensor Fusion Approach for Diagnosing Electrical and Mechanical Faults in Induction Motors," in IEEE Transactions on Industrial Electronics, vol. 66, no. 12, pp. 9510-9520, Dec. 2019.

[14] A. Secic, M. Krpan and I. Kuzle, "Vibro-Acoustic Methods in the Condition Assessment of Power Transformers: A Survey," in IEEE Access, vol. 7, pp. 83915-83931, 2019.

[15] Khazaee M, Ahmadi H, Omid M, Moosavian A, Khazaee M. "Classifier fusion of vibration and acoustic signals for fault diagnosis and classification of planetary gears based on Dempster–Shafer evidence theory," Proceedings of the Institution of Mechanical Engineers, Part E: Journal of Process Mechanical Engineering. 2014;228(1):21-32.

[16] J. Wang, P. Fu, L. Zhang, R. X. Gao and R. Zhao, "Multilevel Information Fusion for Induction Motor Fault Diagnosis," in IEEE/ASME Transactions on Mechatronics, vol. 24, no. 5, pp. 2139-2150, Oct. 2019.

[17] C. Zhao, B. Tang, Y. Huang and L. Deng, "Edge Collaborative Compressed Sensing in Wireless Sensor Networks for Mechanical Vibration Monitoring," in IEEE Transactions on Industrial Informatics, vol. 19, no. 8, pp. 8852-8864, Aug. 2023.

[18] T. Xie, X. Huang and S. -K. Choi, "Intelligent Mechanical Fault Diagnosis Using Multisensor Fusion and Convolution Neural Network," in IEEE Transactions on Industrial Informatics, vol. 18, no. 5, pp. 3213-3223, May 2022.

[19] Non-destructive testing-Acoustic emission inspection-Secondary calibration of acoustic emission sensors, ISO 12714:1999.

[20] Methods for the calibration of vibration and shock transducers - Part 21: Vibration calibration by comparison to a reference transducer, ISO 16063-21:2003.

[21] Y. Luo, J. Gao, P. Chen, L. Hu, Y. Shen and L. Ruan, "A test method of winding deformation excited by pseudorandom M-Sequences — Part I: Theory and simulation," in IEEE Transactions on Dielectrics and Electrical Insulation, vol. 23, no. 3, pp. 1605-1612, June 2016.

[22] Z. Zhang et al., "A Novel IEPE AE-Vibration-Temperature-Combined Intelligent Sensor for Defect Detection of Power Equipment," in IEEE Transactions on Instrumentation and Measurement, vol. 72, pp. 1-9, 2023, Art no. 9506809.

[23] Janů P, Bajer J, Dyčka P, et al. "Precise experimental determination of electrical equivalent circuit parameters for ultrasonic piezoelectric ceramic transducers from their measured characteristics," Ultrasonics, 2021, 112: 106341.